ADVANCED MATERIALS TECHNOLOGIES
www.advmattechnol.de

Noise-Reduced WSe_2 Phototransistors for Enhanced Photodetection Performance via Suppression of Metal-Induced Gap States

Sunggyu Ryoo, Jinwoo Sim, Seungjun Jeong, Juntae Jang, Jaeyong Woo, Jaehyoung Park, Seongmin Ko, Yeeun Kim, Youngmin Song, Jongeun Yoo, Heebeom Ahn, Keehoon Kang, Daeheum Cho, Kyungjune Cho, and Takhee Lee**

Phototransistors are critical components in optoelectronics, and 2D transition metal dichalcogenides (TMDC), such as tungsten diselenide (WSe_2), show promise for phototransistor applications due to their strong light-matter interaction, unique excitonic properties, and high surface-to-volume ratio. In 2D TMDC-based phototransistors, 1/f noise, caused by complex defect states, acts as a dominant low-frequency noise (LFN) and is crucial for obtaining accurate photodetection characteristics. However, many studies still overlook LFN and focus on enhancing photocurrent or response time. In this study, the importance of LFN analysis is highlighted in WSe_2 phototransistors and demonstrate reduced noises and enhanced photodetection performance through the suppression of metal-induced gap states (MIGS) that act as noise sources by utilizing semimetal bismuth (Bi) contact. The WSe_2 phototransistors demonstrated ≈1000 times lower noise, 100 times higher responsivity, and 10 times higher specific detectivity than devices with conventional metal contacts. The results of this study suggest that reducing LFN in photodetection devices, such as by suppressing MIGS, can be an efficient way to enhance device performance.

1. Introduction

Phototransistors are essential in optoelectronics, playing a crucial role in applications such as imaging sensors, optical communication systems, and machine vision technology.[1–5] 2D transition metal dichalcogenides (TMDC) are good candidates for phototransistor applications, exhibiting strong light-matter interaction, interesting excitonic properties, and a high surface-to-volume ratio.[1,6–12] A high-performance phototransistor must possess several key capabilities. It should have high responsivity (R) which is the ratio of optical signals-to-photocurrent conversion; high specific detectivity (D^*) which is the ability to distinguish optical signals from noise sensitively; and fast response time (τ) which refers to how quickly the photocurrent responds to an optical signal.[7]

S. Ryoo, J. Sim[+], J. Jang, J. Woo, J. Park, S. Ko, Y. Kim, Y. Song, J. Yoo, T. Lee
Department of Physics and Astronomy
and Institute of Applied Physics
Seoul National University
Seoul 08826, South Korea
E-mail: tlee@snu.ac.kr

S. Jeong, D. Cho
Department of Chemistry and Green-Nano Materials Research Center
Kyungpook National University
Daegu 41566, South Korea

The ORCID identification number(s) for the author(s) of this article can be found under https://doi.org/10.1002/admt.202500064

[+]Present address: Department of Electrical Engineering and Computer Science, Massachusetts Institute of Technology, 77 Massachusetts Avenue, Cambridge, MA 02139, USA

[Correction added on January 27, 2025, after first online publication: the thirteenth author's affiliation has been adjusted in this version.]

DOI: 10.1002/admt.202500064

H. Ahn
Department of Materials Science and Engineering
and Research Institute of Advanced Materials
Seoul National University
Seoul 08826, South Korea

H. Ahn
Department of Materials Science & Metallurgy
University of Cambridge
27 Charles Babbage Road, Cambridge CB3 0FS, UK

K. Kang
Department of Materials Science and Engineering
Research Institute of Advanced Materials
Institute of Applied Physics
Seoul National University
Seoul 08826, South Korea

K. Cho
Convergence Research Center for Solutions to Electromagnetic Interference in Future-Mobility
Korea Institute of Science and Technology
Seoul 02792, South Korea
E-mail: kcho@kist.re.kr

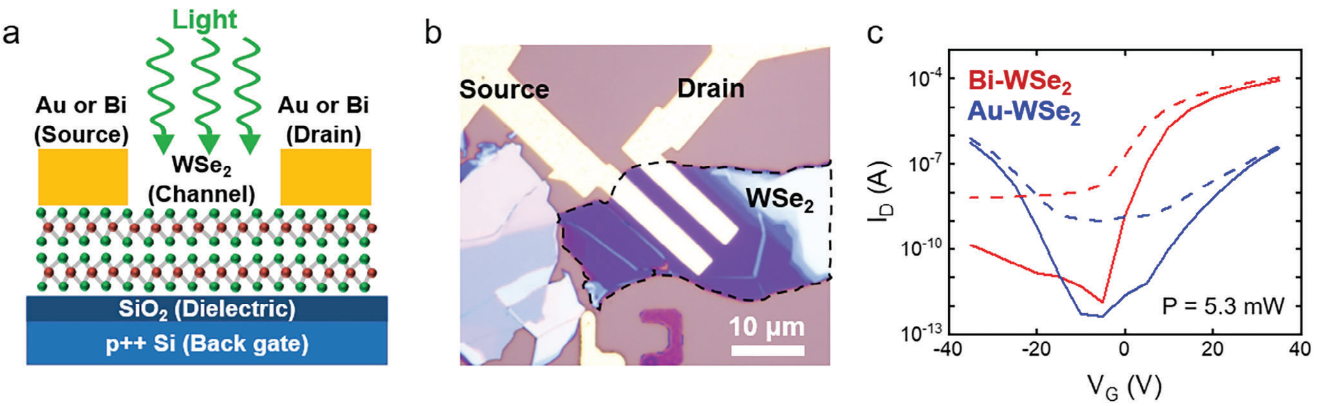

Figure 1. a) Schematic and b) OM image of the WSe_2 phototransistor. c) Transfer characteristics of WSe_2 phototransistors for Au and Bi contacts. The solid lines represent the current under dark conditions, while the dashed lines indicate the current under illumination with 5.3 mW light.

In TMDC-based phototransistors, both photocurrent and noise should be considered for accurate characterization of photodetection performance. However, researchers often make the mistake of considering shot noise which can be easily calculated from dark current as the main noise, without considering 1/f noise which is actually the main noise but requires noise analysis. Also, based on this mistake, most efforts to improve phototransistor performance have been focused solely on enhancing photocurrent and reducing dark current.

In 2D materials, the surface-to-volume ratio is significantly high, causing 2D-based devices to be greatly influenced by electrode contact. Specifically, the inevitable metal-semiconductor contacts in phototransistors often form metal-induced gap states (MIGS) which increase the noise level by acting as noise sources as well as decrease the current level by forming the Schottky barrier.[13–16] In TMDC-based phototransistors, the formation of MIGS negatively impacts photodetection performance from both noise and current perspectives. Several recent studies have reported that semimetal-semiconductor contacts effectively reduce MIGS due to their unique properties of the density of states, which approaches zero near the Fermi level, and we realized this can be another strategy for enhancing photodetection performance.[13–15]

Our study improved the photodetection performance of 2D tungsten diselenide (WSe_2) phototransistors by reducing noise via suppressing MIGS acting as noise sources. We applied semimetal bismuth (Bi) as the electrode to suppress MIGS. We fabricated Au-contact and Bi-contact WSe_2 phototransistors and compared their noise, electrical, and optoelectrical properties. In particular, we employed low-frequency noise analysis to assess contact quality and achieve precise specific detectivity. Our Bi-contact WSe_2 phototransistors showed decreased noise and increased photocurrent compared to devices with conventional Au contacts due to suppression of MIGS. This led to improved overall photodetection performance such as three times faster response time, 100 times higher responsivity, and 10 times enhanced specific detectivity for devices with Bi contacts.

2. Results and Discussion

2.1. Basic Characterization of WSe_2 Transistors

We used mechanically exfoliated WSe_2 flakes as the transistor channel. After making patterns on the flakes with e-beam lithography, electrode materials such as Au and Bi were deposited to fabricate the WSe_2 transistors (Figure S1, Supporting Information). The Raman spectrum confirmed that the WSe_2 flakes used for transistors are a multilayered structure, consistent with the atomic force microscopy characterization (Figure S2, Supporting Information).[17,18] **Figure 1a** shows a device schematic of WSe_2 phototransistors, and Figure 1b shows an optical image of a completed device. To understand the basic electrical properties of the devices, we measured the transfer characteristics (drain current versus gate voltage; I_D-V_G). As shown in Figure 1c, the Au-contacted device exhibits ambipolar behavior. On the other hand, the device with Bi contact shows the n-type characteristics due to the low work function of the Bi.[13] We also measured the output characteristics (drain current versus drain voltage; I_D-V_D) for Au- and Bi-contact devices (Figures S3 and S4, Supporting Information). The Bi-contact device exhibited a clear ohmic behavior, whereas the Au-contact device did not.

2.2. Low-Frequency Noise Analysis of WSe_2 Phototransistors

In 2D TMDC, the primary noise sources are shot noise and 1/f noise.[19,20] Shot noise, arising from thermal fluctuations and the discrete nature of carriers, can be readily calculated by dark current and has been widely regarded as the main noise source in many phototransistor studies. Especially, shot noise can be obtained by the following equation $i_{N,\,shot} = \sqrt{2eI_D\Delta f}$, where e is the elementary charge, I_D is dark current, and Δf is the bandwidth.[7] However, in phototransistors based on 2D materials, the primary noise source is 1/f noise, which is known to arise from complex defect states.[19,20] Unlike shot noise which can be calculated with only the dark current, obtaining 1/f noise requires low-frequency noise (LFN) analysis.[5]

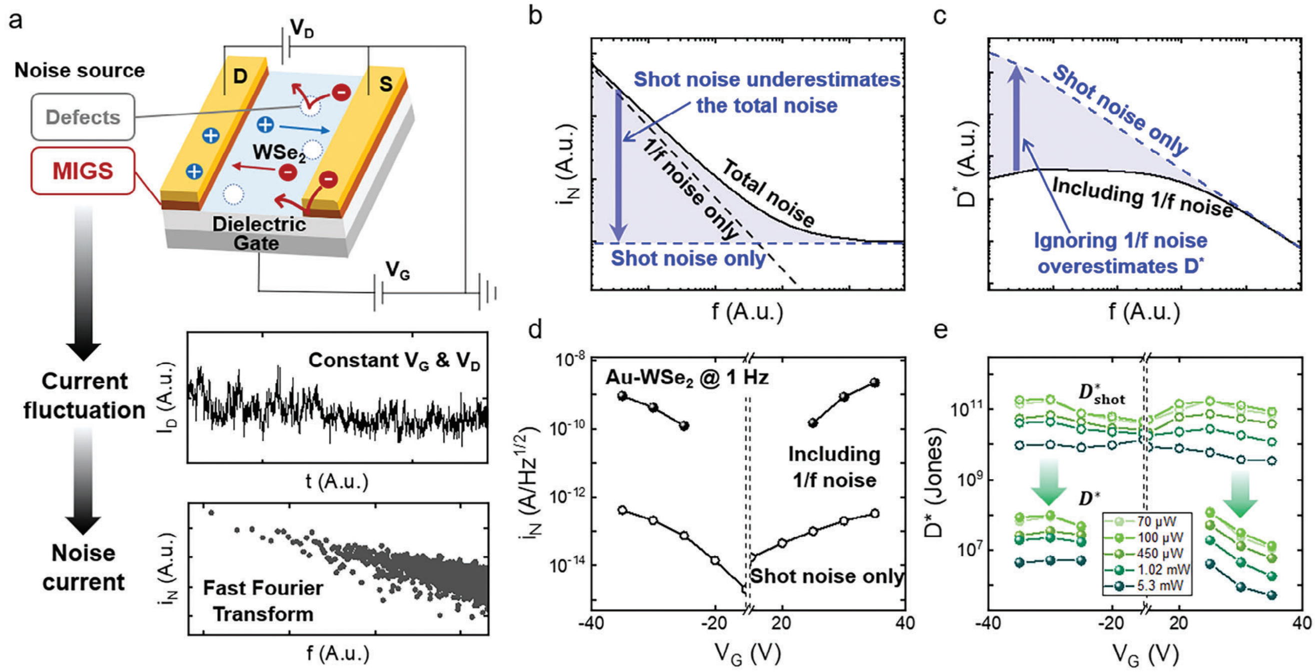

Figure 2. a) Schematic illustration of low-frequency noise (LFN) analysis. Scenarios of b) noise and c) specific detectivity characteristics for TMDC-based phototransistors. d) Noise and e) specific detectivity characteristics for Au-contact WSe_2 phototransistors at a bandwidth of 1 Hz.

We performed LFN analysis to accurately characterize the WSe_2 phototransistors. **Figure 2a** illustrates the process of LFN analysis. The primary noise sources in 2D TMDC are channel defects and metal-induced gap states (MIGS) at the contact. Carriers are trapped and detrapped in contact and channel defects, leading to fluctuations in the current (see schematic in Figure 2a top).[16] Analyzing current fluctuations using a fast Fourier transform (FFT) yields the distribution of noise current (i_N) in the frequency domain. Thus, LFN analysis offers valuable insights into the contact quality of the device.

Figure 2b shows a scenario for TMDC-based phototransistors, demonstrating that considering only shot noise underestimates the total noise. Shot noise is significant only in high-frequency ranges, such as in ultrafast phototransistors. In particular, underestimated noise leads to an overestimation of specific detectivity that can be obtained by the following equation $D^* = R\sqrt{A\,\Delta f}/i_N$, where A is the area of a photosensitive area and i_N is the noise current (see Figure 2c).[19] Figure 2d compares the noise currents measured in WSe_2 transistors considering only shot noise and both shot and 1/f noises, clearly showing higher noise currents when including 1/f noise. Note that the noise profile follows the current profile, as a higher carrier flow increases the frequency of trapping and detrapping events in MIGS and defects. Then, Figure 2e compares the specific detectivity values (D^*_{shot}) of WSe_2 phototransistors for various light intensities by considering only shot noise and those (D^*) by considering both shot and 1/f noises, confirming that specific detectivity is indeed overestimated when only shot noise is considered. For example, at a 1 Hz bandwidth, shot noise was ≈1000 times smaller than 1/f noise, leading to an overestimation of specific detectivity by ≈1000 times. Thus, accurately measuring noise through LFN analysis is crucial for phototransistor study.

2.3. Optoelectric Characterization of WSe_2 Phototransistors

To examine the optoelectrical properties of the WSe_2 phototransistors, a 532 nm laser was used. The current through the device was measured by varying both the laser intensity and the gate voltage. The transfer characteristics of Bi-contact WSe_2 phototransistors are shown in **Figure 3a** as a function of laser intensity. Also, the WSe_2 phototransistor exhibited a clear and fast photoswitching behavior, with a switching speed on the scale of milliseconds (Figures 3b and S5, Supporting Information).

Figure 3c displays the responsivity of the Bi-contact WSe_2 phototransistors. Responsivity, defined as the ratio of incident light to generated photocurrent, is calculated from $R = I_{ph}/P_{eff}$, where photocurrent (I_{ph}) is determined as the difference between the currents under illuminated and dark conditions and effective power (P_{eff}) refers to the power incident on the photosensitive area.[7] The trend of increasing responsivity with higher gate voltage can be explained by the photogating effect (PGE). The photogeneration mechanism in TMDC-based phototransistors is divided into the photoconductive effect (PCE) and the PGE.[1,5] In PCE which converts incident light directly into photocurrent, the photocurrent and power have a proportional relationship, following $I_{ph} \sim P^1$. In contrast, the PGE, where some carriers provide an additional gating effect, exhibits a nonlinear relationship, expressed as $I_{ph} \sim P^{\alpha}$ ($0 < \alpha < 1$). Since the PGE increases the photocurrent level, a higher gate voltage that amplifies the

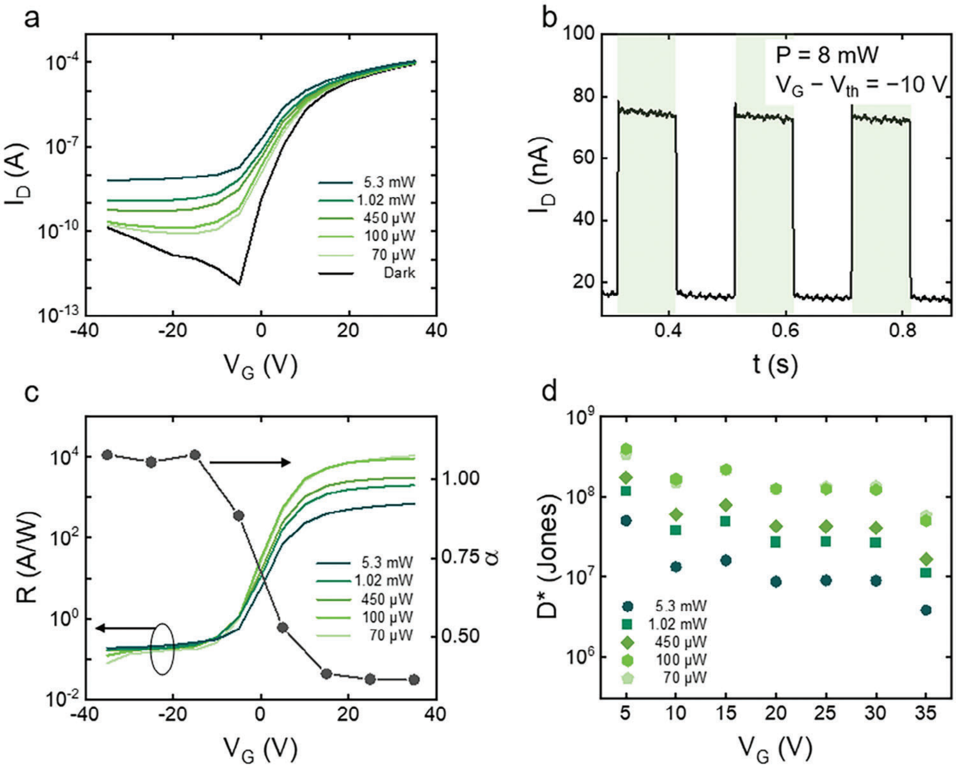

Figure 3. a) Transfer curves and b) photoresponses of Bi-contact WSe_2 phototransistors. Gate dependence of c) the responsivity, the α, and d) the specific detectivity of Bi-contact WSe_2 phototransistors.

dominance of PGE results in a decrease in α and an increase in responsivity.[5] Explaining the gate and power dependences of the responsivity through the PGE is also valid for Au-contact devices (Figure S6, Supporting Information). An important observation is that the Au-contact phototransistor exhibits a stronger PGE compared to the Bi-contact phototransistor. Since the contact material is the only differing factor, this suggests that the gap states in the Au-WSe_2 junction trap carriers more effectively. Consequently, this indicates that Bi has a lower density of gap states than Au, indirectly revealing a difference in MIGS between the two contact materials.

Figure 3d shows the specific detectivity of the Bi-contact WSe_2 phototransistors considering both 1/f and shot noises. As mentioned in the previous section, we used LFN analysis to obtain accurate noise current, enabling precise specific detectivity calculation. Specific detectivity is determined by responsivity and noise current, allowing its trend to be explained through the individual tendencies of these two quantities. As mentioned earlier, responsivity increases with higher gate voltage due to the stronger PGE. The noise current tends to increase as the current grows, which can be attributed to a higher number of carriers leading to more frequent trapping and detrapping events in gap states. However, as the carrier concentration rises, the contribution of excess noise to the total noise becomes more significant.[16] Considering that responsivity is proportional to the photocurrent, this behavior of the noise current effectively explains the slight decrease in specific detectivity as the gate voltage increases.

2.4. Enhanced Performance of WSe_2 Phototransistors with Semimetal Contact

Figure 4 compares the noise, electrical, and optoelectrical properties of the WSe_2 phototransistors with Au and Bi contacts. Note that we conducted well-controlled experiments to eliminate various factors that could influence the device properties except contact materials, such as the device geometry or fabrication. Additionally, the photoresponse and noise characteristics as a function of WSe_2 thickness are presented in Figures S8 and S9 (Supporting Information). For precise comparison between the two types of devices, measurements were conducted at the same overdrive voltage (V_G–V_{th}, V_{th} is a threshold voltage).[5] Figure 4a shows the output characteristics of the WSe_2 phototransistors with Au and Bi contacts. It was observed that the Bi-contact device exhibited a current level approximately 500 times higher than the Au-contact device. Additionally, unlike the Schottky behavior with a curved output characteristic observed in the Au-contact device, the Bi-contact device exhibited fully ohmic characteristics. This is because, as previously explained, MIGS that induce a Schottky barrier in metal contacts are significantly reduced in semimetal contacts.[13,14] The reduction in MIGS decreases the rate of carrier trapping and detrapping, resulting in improved response time and reduced noise. In Figure 4b,c, we observed that the response time decreased by ≈3 times and the normalized noise decreased by ≈1000 times with Bi-contact devices. In both Au- and Bi-contact devices, the noise current exhibits the $1/f^{\gamma}$

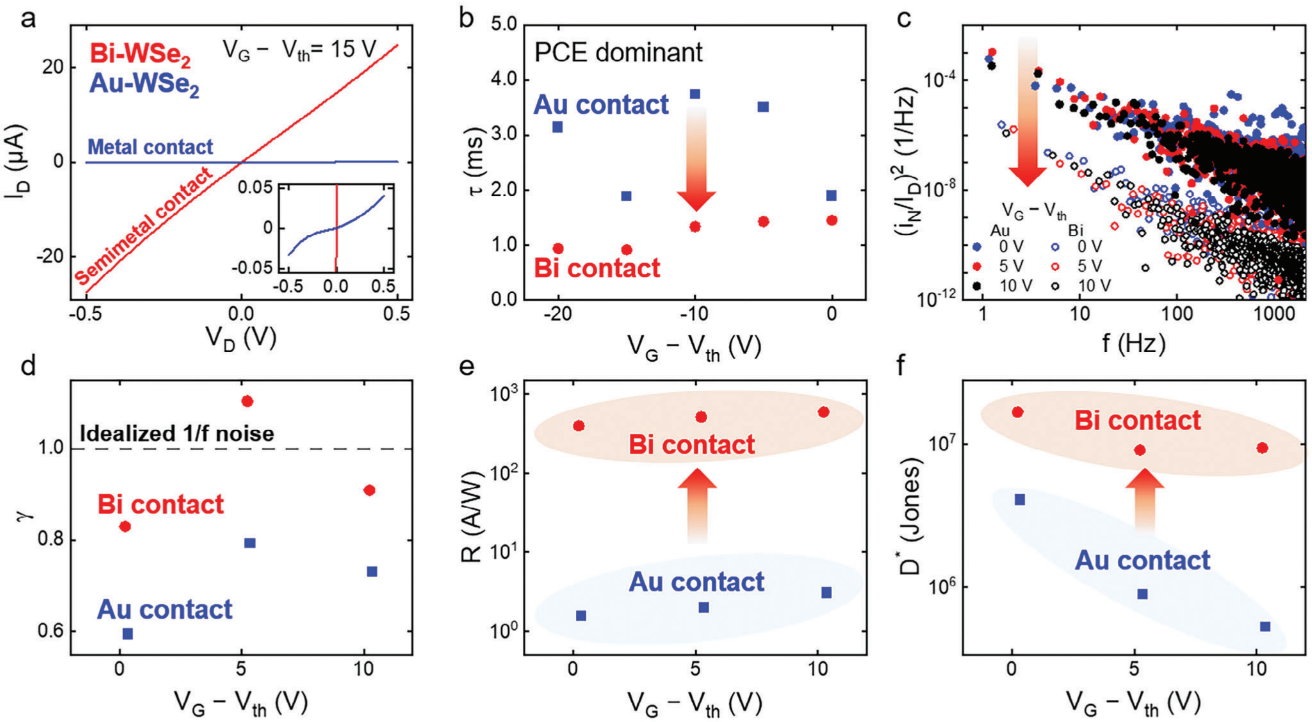

Figure 4. a) Output characteristics (inset: magnified output curve), b) response time, c) normalized noise, d) noise slope γ, e) responsivity, and f) specific detectivity of WSe_2 phototransistors with Au and Bi contacts.

behavior, so we can evaluate how close the noise was to the ideal 1/f noise by examining the noise slope (γ). As shown in Figure 4d, Bi-contact devices are much closer to the ideal 1/f noise current ($\gamma = 1$) than Au-contact devices. This result further emphasizes the impact of high-quality contact properties achieved by the suppression of MIGS.[16]

Achieving good contact properties through reduced MIGS led to improved phototransistor performance metrics. The reduction of MIGS density suppresses the Schottky barrier, enhancing carrier injection and photocurrent, ultimately resulting in increased responsivity. As shown in Figure 4e, responsivity improved ≈100 times across all gate voltage ranges with Bi-contact devices. Additionally, as the MIGS acting as a noise source was reduced, normalized noise decreased significantly. This, combined with the improved responsivity, creates a synergistic effect that enhances specific detectivity (Figure 4f). Bi-contact devices also exhibited great stability under ambient air conditions (Figure S10, Supporting Information).

Figure 5a,b illustrate the mechanisms of performance enhancement through the projected local density of states and band diagrams. As shown in Figure 5a, when a conventional metal like Au forms a junction with WSe_2, both the conduction and valence bands of the semiconductor contribute to the formation of MIGS, leading to Fermi-level pinning and the creation of a Schottky barrier. In contrast, when a semimetal like Bi forms a junction with WSe_2, only the valence band contributes to MIGS formation, resulting in MIGS below the Fermi level and enabling gap-state saturation.[13] Consequently, MIGS are reduced, and an ohmic contact is formed in the Bi-WSe_2 contact. This discussion is well-known and generally applicable to other semimetal-TMDC junctions (Table S1, Supporting Information). The differences between these two contacts become pronounced when applied to a phototransistor (Figure 5b). In the case of conventional metal contact, photogenerated carrier injection is limited, resulting in a lower current level, while carriers trapped and detrapped in MIGS contribute to increased noise. In contrast, semimetal contact allows efficient carrier injection, resulting in higher current levels, while suppressing LFN. Enhanced carrier injection improves responsivity, while the reduced MIGS enhances response time and specific detectivity.

As a result, by suppressing the MIGS, we can enhance photodetection performance and achieve significantly superior performance compared to previously reported TMDC-based photodetectors. Figure 5c,d compare various studies on MoS_2 and WSe_2-based phototransistors concerning key performance metrics: response time, responsivity, and specific detectivity. Note that, ideally, it would be best to compare specific detectivities based on accurate 1/f noise analysis. However, due to the limited number of such studies, we compared the specific detectivity based on shot noise, as most researchers commonly do. Specific performance metrics for the devices shown in Figure 5c,d can be found in Table S2 (Supporting Information). Figure 5c,d show that the performance of our Bi-contact WSe_2 phototransistors is positioned closer to the desired corner (fast response time, high responsivity, and high specific detectivity; marked as orange boxes) than the Au-contact devices. Only devices labeled 5,[21] 6,[4] and 9[22] were closer to the desired corner than our Bi-contact devices; however, these rely on entirely different mechanisms, such as avalanche breakdown or

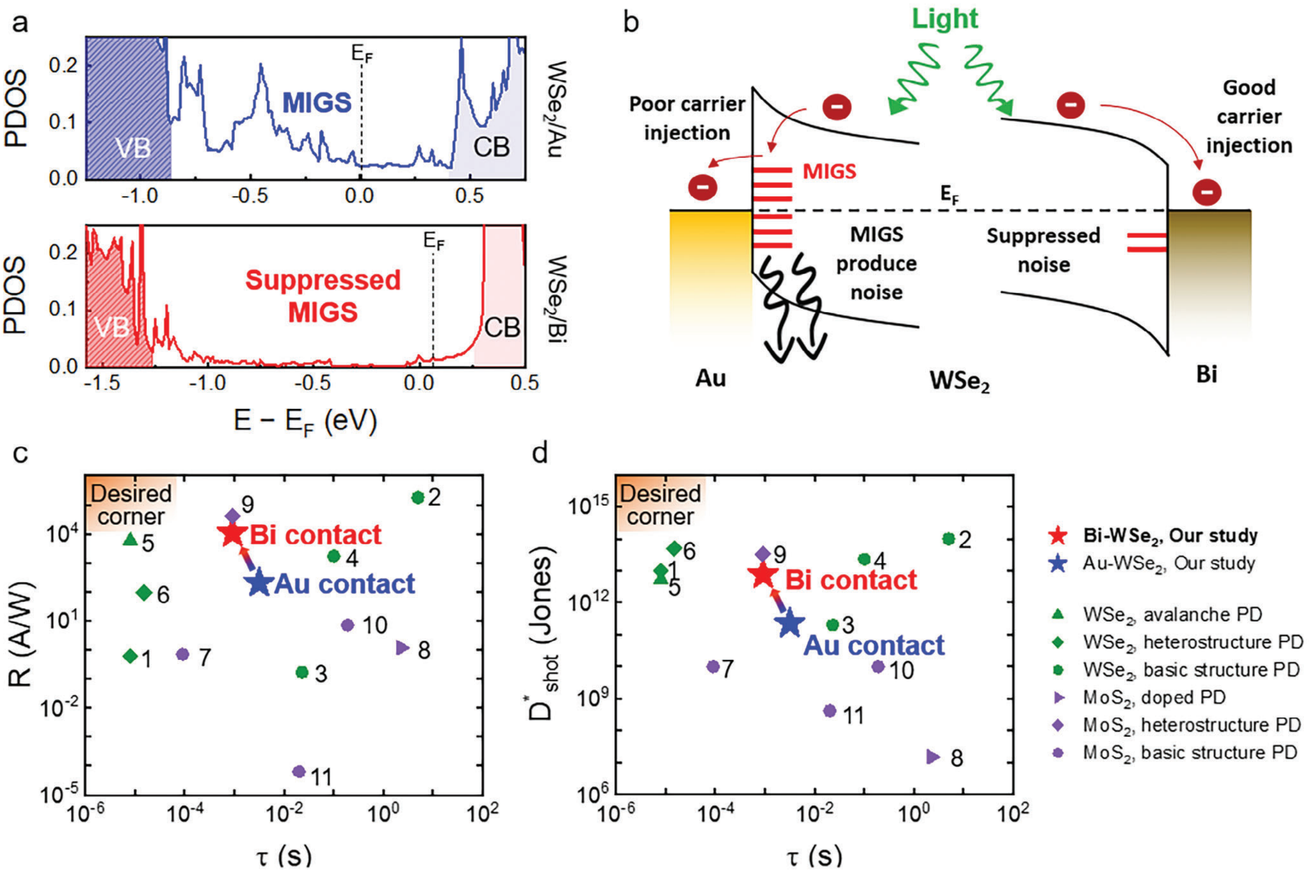

Figure 5. a) Projected density of states calculations for WSe_2/Bi and WSe_2/Au junctions. b) The band diagram of the Au-contact WSe_2 and the Bi-contact WSe_2 phototransistors. The red line represents the MIGS and the black wavy arrow represents the noise generated by MIGS. c) Responsivity and d) specific detectivity versus response time for WSe_2 and MoS_2-based photodetectors (devices labeled as 1,[23] 2,[24] 3,[24] 4,[25] 5,[21] 6,[4] 7,[26] 8,[27] 9,[22] 10,[28] and 11[29]).

heterostructures. Excluding specialized photodetectors that use techniques like avalanche breakdown or heterostructures, our Bi-contact device demonstrates the best performance among devices with a basic structure. Furthermore, our device showed superior performance compared to photodetectors made of perovskite or organic materials (Table S3, Supporting Information).

3. Conclusion

This study demonstrates the enhanced photodetection performance of WSe_2 phototransistors. By reducing metal-induced gap states, Bi-contact WSe_2 phototransistors facilitate improved carrier injection, lowered noise levels, and enhanced key performance metrics such as responsivity, specific detectivity, and response time. Low-frequency noise analysis provided accurate noise characterization, offering valuable insights into contact properties and enabling precise specific detectivity calculations, further validating the advantages of Bi contacts over conventional metal contacts such as Au. Our results show that this approach maintains the thin and flexible nature of 2D materials, allowing for high-performance photodetection in a straightforward configuration without requiring complex processing steps.

4. Experimental Section

Fabrication of WSe_2 Phototransistors: WSe_2 flakes were mechanically exfoliated from bulk crystals and transferred on a 270 nm SiO_2/p++ Si substrate, with flake selection and thickness measurement conducted using an optical microscope and an atomic force microscopy (AFM) system (NX-10, Park Systems). After spin-coating of methyl methacrylate and poly methyl methacrylate resist layers on the WSe_2 flakes, source and drain electrodes were patterned using an electron-beam lithography system (JSM-6510, JEOL0). A 40 nm Au layer was deposited as electrodes using an electron-beam evaporator (KVE2004 L, Korea Vacuum Tech) for the Au-contacted phototransistors. For the Bi-contact phototransistors, a 20 nm Bi layer was first deposited using a thermal evaporator (KVE-T2000, Korea Vacuum Tech), and then a 40 nm Au layer was deposited.

Optical and Electrical Characterization: The photoluminescence (PL) and Raman spectra were obtained through a confocal imaging system (Xper Raman 200, Nanobase) with an incident laser beam of wavelength 532 nm. The electrical characteristics and low-frequency noise analysis of phototransistors were measured by using a probe station (M6VC, MSTECH) and a semiconductor parameter analyzer (Keithley 4200). The photoresponses of phototransistors were measured under laser (MDE5240 V) illumination of wavelength 532 nm. The laser beam was globally illuminated to phototransistors with a few millimeters in diameter. All of the characterizations were performed at room temperature and in an N_2 environment (500 Torr) for stable device operation and to shield the phototransistors from degrading factors such as humidity and various gases in the air.

Computational Calculations: The electronic structure calculations were performed through density functional theory (DFT) within the Perdew–Burke–Ernzerhof (PBE) functional framework, as implemented in the Vienna Ab initio Simulation Package (VASP 6.4.0).

Supporting Information

Supporting Information is available from the Wiley Online Library or from the author.

Acknowledgements

The authors appreciate the financial support of the National Research Foundation of Korea (NRF) grant (No. 2021R1A2C3004783 and No. RS-2023-00220471), the Brain Link program (No. 2022H1D3A3A01077343), and the Nano•Material Technology Development Program grant (No. 2021M3H4A1A02049651) through NRF funded by the Ministry of Science and ICT of Korea, and the industry–university cooperation program by Samsung Electronics Co., Ltd. (IO201211-08047-01). K.C. acknowledges the National Research Council of Science & Technology (NST) grant (CRC22031-000).

Conflict of Interest

The authors declare no conflict of interest.

Data Availability Statement

The data that support the findings of this study are available in the supplementary material of this article.

Keywords

low-frequency noise, metal-induced gap states, phototransistors, semimetal, transition metal dichalcogenides

Received: January 10, 2025
Published online: January 23, 2025

[1] J. O. Island, S. I. Blanter, M. Buscema, H. S. J. Van Der Zant, A. Castellanos-Gomez, *Nano Lett.* **2015**, *15*, 7853.
[2] T. Dong, J. Simões, Z. Yang, *Adv. Mater. Interfaces* **2020**, *7*, 1901657.
[3] H.-L. Sinn, A. Kumar, E. Pop, A. Newaz, *Adv. Photonics Res.* **2023**, *4*, 2300029.
[4] S. Ghosh, A. Varghese, K. Thakar, S. Dhara, S. Lodha, *Nat. Commun.* **2021**, *12*, 3336.
[5] J. Sim, S. Ryoo, J. S. Kim, J. Jang, H. Ahn, D. Kim, J. Jung, T. Kong, H. Choi, Y. S. Lee, T. W. Lee, K. Cho, K. Kang, T. Lee, *ACS Nano* **2024**, *18*, 16905.
[6] J. Jiang, Y. Wen, H. Wang, L. Yin, R. Cheng, C. Liu, L. Feng, J. He, *Adv. Electron. Mater.* **2021**, *7*, 2001125.
[7] M. Long, P. Wang, H. Fang, W. Hu, *Adv. Funct. Mater.* **2019**, *29*, 1803807.
[8] Q. H. Wang, K. Kalantar-Zadeh, A. Kis, J. N. Coleman, M. S. Strano, *Nat. Nanotechnol.* **2012**, *7*, 699.
[9] W. Seo, W. Park, H. Y. Seo, S. Oh, O. Kwon, S. H. Jeong, D. H. Kim, M. J. Kim, S. K. Lee, B. H. Lee, B. Cho, *Appl. Surf. Sci.* **2022**, *604*, 154485.
[10] L. Kuo, V. K. Sangwan, S. V. Rangnekar, T. C. Chu, D. Lam, Z. Zhu, L. J. Richter, R. Li, B. M. Szydłowska, J. R. Downing, B. J. Luijten, L. J. Lauhon, M. C. Hersam, *Adv. Mater.* **2022**, *34*, 2203772.
[11] H. Kim, S. Z. Uddin, N. Higashitarumizu, E. Rabani, A. Javey, *Science* **2021**, *373*, 448.
[12] Y. Miyamoto, D. Yoshikawa, K. Takei, T. Arie, S. Akita, *Jpn. J. Appl. Phys.* **2018**, *57*, 06HB01.
[13] P. C. Shen, C. Su, Y. Lin, A. S. Chou, C. C. Cheng, J. H. Park, M. H. Chiu, A. Y. Lu, H. L. Tang, M. M. Tavakoli, G. Pitner, X. Ji, Z. Cai, N. Mao, J. Wang, V. Tung, J. Li, J. Bokor, A. Zettl, C. I. Wu, T. Palacios, L. J. Li, J. Kong, *Nature* **2021**, *593*, 211.
[14] W. Li, X. Gong, Z. Yu, L. Ma, W. Sun, S. Gao, Ç. Köroğlu, W. Wang, L. Liu, T. Li, H. Ning, D. Fan, Y. Xu, X. Tu, T. Xu, L. Sun, W. Wang, J. Lu, Z. Ni, J. Li, X. Duan, P. Wang, Y. Nie, H. Qiu, Y. Shi, E. Pop, J. Wang, X. Wang, *Nature* **2023**, *613*, 274.
[15] H. Yu, H. Zeng, Y. Zhang, Y. Liu, W. ShangGuan, X. Zhang, Z. Zhang, Y. Zhang, *Adv. Funct. Mater.* **2025**, *35*, 2412913.
[16] W. Shin, J. Byeon, R. H. Koo, J. Lim, J. H. Kang, A. R. Jang, J. H. Lee, J. J. Kim, S. N. Cha, S. Pak, S. T. Lee, *Adv. Sci.* **2024**, *11*, 2307196.
[17] H. Li, G. Lu, Y. Wang, Z. Yin, C. Cong, Q. He, L. Wang, F. Ding, T. Yu, H. Zhang, *Small* **2013**, *9*, 1974.
[18] J. Seo, K. Cho, W. Lee, J. Shin, J. K. Kim, J. Kim, J. Pak, T. Lee, *Nanoscale Res. Lett.* **2019**, *14*, 313.
[19] F. Wang, T. Zhang, R. Xie, Z. Wang, W. Hu, *Nat. Commun.* **2023**, *14*, 2224.
[20] A. Rogalski, *Nat. Nanotechnol.* **2022**, *17*, 217.
[21] L. Gao, N. Zhang, J. You, B. Wang, B. Zhang, Z. Han, Z. Jiang, T. Miao, H. Guo, J. Zhang, H. Hu, L. Wang, *ACS Photonics* **2023**, *10*, 4349.
[22] C. Wang, Q. Wu, Y. Ding, X. Zhang, W. Wang, X. Guo, Z. Ni, L. Lin, Z. Cai, X. Gu, S. Xiao, H. Nan, *ACS Appl. Mater. Interfaces* **2023**, *15*, 46236.
[23] T. Wang, K. Andrews, A. Bowman, T. Hong, M. Koehler, J. Yan, D. Mandrus, Z. Zhou, Y. Q. Xu, *Nano Lett.* **2018**, *18*, 2766.
[24] W. Zhang, M. H. Chiu, C. H. Chen, W. Chen, L. J. Li, A. T. S. Wee, *ACS Nano* **2014**, *8*, 8653.
[25] D. Wang, C. Tan, H. Wu, L. Yang, Z. Wang, *Appl. Phys. Lett.* **2024**, *124*, 011103.
[26] D. S. Tsai, K. K. Liu, D. H. Lien, M. L. Tsai, C. F. Kang, C. A. Lin, L. J. Li, J. H. He, *ACS Nano* **2013**, *7*, 3905.
[27] S. H. Yu, Y. Lee, S. K. Jang, J. Kang, J. Jeon, C. Lee, J. Y. Lee, H. Kim, E. Hwang, S. Lee, J. H. Cho, *ACS Nano* **2014**, *8*, 8285.
[28] H. Yan, J. Cheng, K. Zhu, A. Li, T. Peng, Y. Luo, *Curr. Appl. Phys.* **2020**, *20*, 643.
[29] Y. Lee, J. Yang, D. Lee, Y. H. Kim, J. H. Park, H. Kim, J. H. Cho, *Nanoscale* **2016**, *8*, 9193.